Applied Microbiology and Biotechnology (2019) 103:1713–1724
https://doi.org/10.1007/s00253-018-9546-8

BIOTECHNOLOGICAL PRODUCTS AND PROCESS ENGINEERING

Morphology engineering for enhanced production of medium-chain-length polyhydroxyalkanoates in *Pseudomonas mendocina* NK-01

Fengjie Zhao[1] · Ting Gong[1] · Xiangsheng Liu[1] · Xu Fan[1] · Rui Huang[1] · Ting Ma[1] · Shufang Wang[2] · Weixia Gao[2] · Chao Yang[1]

Received: 7 October 2018 / Revised: 23 November 2018 / Accepted: 27 November 2018 / Published online: 4 January 2019

Abstract

Polyhydroxyalkanoates (PHAs) can be produced by microorganisms from renewable resources and are regarded as promising bioplastics to replace petroleum-based plastics. A medium-chain-length PHAs (mcl-PHA)-producing strain *Pseudomonas mendocina* NK-01 was isolated previously by our lab and its whole-genome sequence is currently available. Morphology engineering of manipulating cell morphology–related genes has been applied for enhanced accumulation of the intracellular biopolymer short-chain-length PHAs (scl-PHA). However, it has not yet been reported to improve the yield of mcl-PHA by morphology engineering so far. In this work, several well-characterized cell morphology–related genes, including the cell fission ring (Z-ring) location genes *minCD*, peptidoglycan degradation gene *nlpD*, actin-like cytoskeleton protein gene *mreB*, Z-ring formation gene *ftsZ*, and FtsZ inhibitor gene *sulA*, were intensively investigated for their impacts on the cell morphology and mcl-PHA accumulation by gene knockout and overexpression in *P. mendocina* NKU, a *upp* knockout mutant of *P. mendocina* NK-01. For a *minCD* knockout mutant *P. mendocina* NKU-Δ*minCD*, the average cell length was obviously increased and the mcl-PHA production was improved. However, the *nlpD* knockout mutant had a shorter cell length and lower mcl-PHA yield compared with *P. mendocina* NKU. Overexpression of *mreB* in *P. mendocina* NKU resulted in spherical cells. When *ftsZ* was overexpressed in *P. mendocina* NKU, the cell division was accelerated and the mcl-PHA titer was improved. Furthermore, *mreB*, *ftsZ*, or *sulA* was overexpressed in *P. mendocina* NKU-Δ*minCD*. Consequently, the mcl-PHA titers were all increased compared with *P. mendocina* NKU-Δ*minCD* carrying the empty vector. The multiple fission pattern was finally achieved in *ftsZ*-overexpressing NKU-Δ*minCD*. In this work, improved production of mcl-PHA in *P. mendocina* NK-01 has been achieved by morphology engineering. This work provides an alternative strategy to enhance mcl-PHA accumulation in mcl-PHA-producing strains.

Keywords *Pseudomonas mendocina* · Morphology engineering · mcl-PHA · Cell morphology–related genes

Introduction

The concept of "morphology engineering" has been recently proposed (Jiang and Chen 2016). Cell morphology has been shown to be associated with cell growth, downstream separation, and inclusion body accumulation (Wang and Lee 1997; Tan et al. 2014). Bacterial cytoskeleton, which consists of actin, tubulin, and inner filaments, and cell division pattern have important functions to maintain the bacterial cell morphology.

Several proteins play important roles in the cell division. A tubulin-like protein, FtsZ, interacts with many other proteins, leading to the formation of Z-ring and completion of cytokinesis (Loose and Mitchison 2014; Margolin 2005; Villanelo et al. 2011; Boyle et al. 1997). SulA, MinC, and MinD

Electronic supplementary material The online version of this article (https://doi.org/10.1007/s00253-018-9546-8) contains supplementary material, which is available to authorized users.

✉ Shufang Wang
wangshufang@nankai.edu.cn

✉ Weixia Gao
watersave@126.com

✉ Chao Yang
yangc20119@nankai.edu.cn

[1] Key Laboratory of Molecular Microbiology and Technology for Ministry of Education, Nankai University, Tianjin 300071, China

[2] State Key Laboratory of Medicinal Chemical Biology, Nankai University, Tianjin 300071, China

function as FtsZ inhibitors, which prevent the formation of Z-ring in various ways (Chen et al. 2012; Bi and Lutkenhaus 1993; Anderson et al. 2004).

The "min" system has an important function for proper localization of Z-ring. MinCD, which blocks the formation of the FtsZ ring at all sites, and MinE, which relieves the division block at the mid-cell site, precisely regulate the cell division in binary fission (Rowlett and Margolin 2013; Ivanov and Mizuuchi 2010). Knockout of genes *minCD* leads to the formation of multiple Z rings in several positions of the cell (Howard 2004; Pichoff and Lutkenhaus 2001). Thus, the pattern of cell division is changed from binary fission to multiple fission and the cell length also becomes several-fold longer than the wild type (Wu et al. 2016a, b). A SOS-inducible protein SulA interacts with FtsZ through GTP hydrolysis to inhibit cell division (Higashitani et al. 1995). Overexpression of SulA in *Escherichia coli* disrupts the Z-ring formation due to inhibition of the assembly of FtsZ in the division ring and SulA-overexpressing cells become filamentary (Dajkovic et al. 2008; Wang et al. 2014). In addition, overexpression of FtsZ in *Escherichia coli* promotes cell division, leading to high cell density and smaller cell size (Wang and Lee 1997; Ward and Lutkenhaus 1985).

During the cell division, the peptidoglycan layer must be split by amidases to be shared by the two daughter cells (den Blaauwen et al. 2008). NlpD can regulate directly the cell division by activating amidases (Uehara et al. 2009, 2010). Knockout of *nlpD* in *E. coli* destroys the function of amidases and thus disrupts the binary fission. An actin-like cytoskeleton protein MreB plays an important role in maintaining cell shape (Gitai 2005; Wang et al. 2010; Cabeen and Jacobs-Wagner 2010; Van den Ent et al. 2001). Previous studies have shown that the cell shape of the *mreB* knockout mutant can be changed from rod to sphere (Jiang et al. 2015, 2017), and that overproduction of MreB can increase the width of the cell (Wu et al. 2016a).

Polyhydroxyalkanoates (PHAs) belong to biopolyesters intracellularly accumulated by a variety of bacteria as carbon and energy storage under unbalanced growth conditions (Reddy et al. 2003; Li et al. 2007). PHAs have been used as potential alternatives to petroleum-based plastics due to their unique properties such as biodegradability, biocompatibility, and excellent thermal and mechanical properties (Chen and Wu 2005; Chen 2009; Gao et al. 2011). PHAs are traditionally classified into two major types based on monomer carbon chain length, i.e., short-chain-length PHAs (scl-PHA) containing monomer units of C3 to C5 and medium-chain-length PHAs (mcl-PHA) containing monomer units of C6 to C14 (Chung et al. 2013; Ma et al. 2009).

However, the production cost of PHAs is higher than that of the petrochemical plastics for many reasons, such as expensive substrate, difficult downstream processing, and small cell sizes. It has been reported that morphology-engineered bacteria with larger cell sizes are capable of accumulating more inclusion bodies, such as PHAs.

After *sulA* overexpression in *E. coli*, the poly(3-hydroxybutyrate) (PHB) content was increased from 12.05 to 26.54 wt.% and the cell dry weight (CDW) was increased from 4.03 to 8.24 g/L (Wang et al. 2014). Weaken expression of *mreB* in *mreB*-deleting *E. coli* resulted in larger cell size and higher PHB accumulation from 53.19 to 73.53 wt.% (Jiang et al. 2015). In combination with inducible expression of *sulA* in the above mutant strain, the PHB accumulation was further improved to 80.41 wt.% and the filamentary cells were generated. Further, CRISPRi (clustered regularly interspaced short palindromic repeats interference) was utilized to regulate expression intensities of *ftsZ* or/and *mreB* in *E. coli*, leading to different cell sizes and increased PHB accumulation (Elhadi et al. 2016). Knockout of *minCD* in *E. coli* JM109 resulted in elongated cells and increased PHB production from 53.22 to 60.23 wt.% (Wu et al. 2016a, b). After *ftsZ*, *mreB*, and *sulA* overexpression in *E. coli* JM109Δ*minCD*, the PHB accumulation was improved to 73.31, 70.51, and 70 wt.%, respectively, and the cell size became larger (Wu et al. 2016a, b). Simultaneous overexpression of FtsZ ring–related genes and *mreB* in *E. coli* JM109Δ*minCD*, the cell growth rate was further increased together with a significant increase in the PHB accumulation up to 82.13 wt.% (Wu et al. 2016a). Not only *E. coli*, morphology engineering for *Halomonas* could also change the cell size and increase the PHA production. Overexpression of *minCD* in *Halomonas* TD08 elongated the cell shape and enhanced the PHB accumulation from 69 to 82 wt.% (Tan et al. 2014). Using a temperature-sensitive plasmid for *mreB* or *ftsZ* expression in *mreB*- or *ftsZ*-deleting *Halomonas campaniensis* LS21 led to increased PHB accumulation from 56.8 to 75.9 or 78.7 wt.% and the formation of larger spherical cells or longer filamentous cells (Jiang et al. 2017). CRISPRi was also used in *Halomonas* TD01 to regulate expression intensities of *ftsZ* to elongate the cell shape (Tao et al. 2017). Therefore, morphology engineering may be a promising approach to improve the production of inclusion bodies.

Many members from the genus *Pseudomonas* have an ability to synthesize mcl-PHA via either β-oxidation pathway or fatty acid de novo biosynthesis pathway. Inhibition of β-oxidation pathway in *Pseudomonas* has been used to synthesize novel mcl-PHA using fatty acids as carbon sources (Chung et al. 2013; Ma et al. 2009; Ouyang et al. 2007; Liu et al. 2011). Metabolic engineering approaches, such as the increase of NADPH availability and the reduction of by-products accumulation, have been used for the improvement of PHA production using glucose as carbon sources through fatty acid de novo biosynthesis (Poblete-Castro et al. 2013; Borrero-de Acuña et al. 2014). However, there is no relevant report about the improvement of mcl-PHA production in microorganisms by applying a morphology engineering strategy so far.

Previously, we isolated a mcl-PHA producing strain *Pseudomonas mendocina* NK-01 from farmland soil, and the biosynthetic pathway of mcl-PHA has been elucidated in this strain (Guo et al. 2011a; Wang et al. 2016). This research aims at investigating the influence of cell morphology on the production of mcl-PHA in *P. mendocina* NK-01. For this purpose, the deletion and overexpression of several cell morphology–related genes were carried out to explore the feasibility of manipulating cell morphology for the improvement of mcl-PHA production in *P. mendocina* NK-01.

Materials and methods

Bacterial strains, plasmids, and growth conditions

Escherichia coli DH5α was used for plasmid construction, and *E. coli* S17-1 was used for conjugal transfer. *Pseudomonas mendocina* NK-01, which was deposited in China Center for Type Culture Collection (CCTCC, no. CCTCC M 208005), is resistant to chloramphenicol and can synthesize mcl-PHA (Guo et al. 2011b). The complete genome sequence of *P. mendocina* NK-01 is available in GenBank under accession number CP002620 (Guo et al. 2011b). *Pseudomonas mendocina* NKU, an *upp* knockout mutant of *P. mendocina* NK-01 (Wang et al. 2015), was used as the starting strain. An *E. coli-Pseudomonas* shuttle vector pBBR1MCS-2 (Kovach et al. 1995) was used to overexpress the cell morphology–related genes. A suicide plasmid pEX18Tc-*upp* (Wang et al. 2015) was used for gene knockout. All plasmids and strains used in this study are listed in Table 1.

Escherichia coli strains were cultivated in Luria-Bertani (LB) medium (Green and Sambrook 2012) at 37 °C. *Pseudomonas mendocina* strains were cultivated in LB medium, nutrient-rich (NR) medium, or PHA fermentation medium (Wang et al. 2016) at 30 °C. When necessary, media were supplemented with chloramphenicol (Cm, 170 μg/mL), tetracycline (Tc, 25 μg/mL), kanamycin (Kan, 50 μg/mL), or 5-fluorouracil (5-FU, 20 μg/mL).

Construction of the gene overexpression plasmids

The *mreB*, *ftsZ*, and *sulA* genes were amplified, respectively, by PCR with the *P. mendocina* NKU genomic DNA as the template. Subsequently, each of the three PCR-generated fragments was inserted into the vector pBBR1MCS-2 via the *Bam*H I restriction site using a homologous recombination kit (Vazyme, Nanjing, China) to construct the overexpression vectors pBBR1MCS-*mreB*, pBBR1MCS-*ftsZ*, and pBBR1MCS-*sulA*, respectively. For construction of pBBR1MCS-*mreB-ftsZ*, the *ftsZ* gene was inserted into the *Xba* I restriction site of the plasmid pBBR1MCS-*mreB* using a homologous recombination kit. The construction processes of the overexpression vectors are shown in Fig. S1.

Construction of the gene knockout mutants

The *minCD* and *nlpD* knockout mutants of *P. mendocina* NKU were constructed based on a scarless genome editing strategy (Wang et al. 2015) using the suicide plasmid in combination with *upp* as a counter-selectable marker. The upstream and downstream homologous arms of *minCD* were amplified, respectively, by PCR with the *P. mendocina* NKU genomic DNA as the template and then ligated together through overlap PCR. The fusion fragment was incorporated into the suicide plasmid pEX18Tc-*upp* to generate the gene targeting vectors pEX18Tc-Δ*minCD*. The construction process of the vector pEX18Tc-Δ*nlpD* was the same as that of the vector pEX18Tc-Δ*minCD* (Fig. 1). The two constructed plasmids were transformed independently into *P. mendocina* NKU using a conjugal transfer procedure described by Wang et al (Wang et al. 2015).

Due to the lack of the replication elements that are functional in *P. mendocina*, the introduced plasmid was forced to integrate via homologous recombination into the chromosome. The single-crossover recombinants were screened by incubating at 30 °C for 24 h on LB agar plates supplemented with 170 μg/mL Cm and 25 μg/mL Tc. Then, the selected recombinants were incubated at 30 °C for 24 h in LB medium. To screen the double-crossover recombinants, the culture broth was diluted to 10^{-2} and spread on LB agar plates supplemented with 20 μg/mL 5-FU. The recombinants showing 5-FU^{r} and Tc^{s} were selected for further validation of the deleted genomic regions by PCR. Finally, the *minCD* and *nlpD* knockout mutants were validated by DNA sequencing. All primers used for plasmid construction and mutant validation are listed in Table S1.

Scanning electron microscopy

After 18 h of incubation, cells were harvested by centrifugation, washed with 0.1 M PBS buffer (pH 7.2) for five times, and fixed overnight with 3% (*v*/*v*) glutaraldehyde. After that, the fixed cells were washed with PBS for five times to remove glutaraldehyde. Subsequently, cells were dehydrated with ethanol using a concentration gradient (*v*/*v*) of 30, 50, 70, 80, 90, and 100% in a sequential way (15 min per concentration). Then, the samples were further dehydrated twice with 100% ethanol and lyophilized in vacuum desiccators. Finally, the samples were coated with gold and observed using a Quanta 200 scanning electron microscope (SEM) (FEI, Hillsboro, USA) for imaging (Feng et al. 2014). The image processing software (Adobe® Photoshop® CC) was used to measure the cell sizes. A minimum of 200 cells per group were measured to get the average cell length and width.

Table 1 Strains and plasmids used in this study

Strains	Description	Source or literature
Strains		
Pseudomonas mendocina NKU	PHA_{MCL} producing strain; Cm^R; preserved in our laboratory; carrying an in-frame deletion in the *upp* gene; starting strain for engineering	This laboratory
P. mendocina NKU-Δ*minCD*	NKU derivative carrying an in-frame deletion in the *minCD* gene	This work
P. mendocina NKU-Δ*nlpD*	NKU derivative carrying an in-frame deletion in the *nlpD* gene	This work
P. mendocina NKU pBBR	NKU derivative containing pBBR1MCS-2; Cm^R; Km^R	This work
P. mendocina NKU pBBR-*mreB*	NKU derivative containing pBBR-*mreB*; Cm^R; Km^R	This work
P. mendocina NKU pBBR-*ftsZ*	NKU derivative containing pBBR-*ftsZ*; Cm^R; Km^R	This work
P. mendocina NKU pBBR-*sulA*	NKU derivative containing pBBR-*sulA*; Cm^R; Km^R	This work
P. mendocina NKU pBBR-*mreB-ftsZ*	NKU derivative containing pBBR-*mreB-ftsZ*; Cm^R; Km^R	This work
P. mendocina NKU-Δ*minCD* pBBR	NKU Δ*minCD* derivative containing pBBR1MCS-2; Cm^R; Km^R	This work
P. mendocina NKU-Δ*minCD* pBBR-*mreB*	NKU Δ*minCD* derivative containing pBBR1MCS-*mreB*; Cm^R; Km^R	This work
P. mendocina NKU-Δ*minCD* pBBR-*ftsZ*	NKU Δ*minCD* derivative containing pBBR1MCS-*ftsZ*; Cm^R; Km^R	This work
P. mendocina NKU-Δ*minCD* pBBR-*sulA*	NKU Δ*minCD* derivative containing pBBR1MCS-*sulA*; Cm^R; Km^R	This work
P. mendocina NKU-Δ*minCD* pBBR-*mreB-ftsZ*	NKU Δ*minCD* derivative containing pBBR1MCS-*mreB-ftsZ*; Cm^R; Km^R	This work
Escherichia coli DH5α	F^-, φ80d*lacZ*ΔM1, Δ(*lacZYA-argF*)U169, *deoR*, *recA*1, *endA*1, *hsdR*17(r_k^-, m_k^+), *phoA*, *supE*44, λ^- *thi*-1, *gyrA*96, *relA*1	This laboratory
E. coli S17-1	*recA*; harbors the *tra* genes of plasmid RP4 in the chromosome; *proA thi-1*	This laboratory
Plasmids		
pBBR1MCS-2	Broad host range; expression plasmid; Km^R; *lacPOZ'*, *mob*	Kovach et al. 1995
pBBR1MCS-*mreB*	pBBR1MCS-2 derivative containing *mreB* gene from NKU; Km^R	This work
pBBR1MCS-*ftsZ*	pBBR1MCS-2 derivative containing *ftsZ* gene from NKU; Km^R	This work
pBBR1MCS-*sulA*	pBBR1MCS-2 derivative containing *sulA* gene from NKU; Km^R	This work
pBBR1MCS-*mreB-ftsZ*	pBBR1MCS-2 derivative containing *mreB and ftsZ* gene from NKU; Km^R	This work
pEX18Tc-*upp*	pEX18Tc derivative, carrying a copy of *upp* gene of *P. mendocina* NKU	This laboratory
pEX18Tc-Δ*minCD*	pEX18Tc-*upp* derivative, carrying the up- and downstream regions of *minCD* gene, used for deletion of the *minCD* gene	This work
pEX18Tc-Δ*nlpD*	pEX18Tc-*upp* derivative, carrying the up- and downstream regions of *nlpD* gene, used for deletion of the *nlpD* gene	This work

Real-time quantitative PCR

Total RNA samples were extracted from the NKU cells using a commercial RNA pure bacteria kit (Cwbio, Beijing, China). After the removal of DNA contamination, cDNA was synthesized by reverse transcription using a HiScript II Q RT SuperMix (Vazyme, Nanjing, China). Real-time PCR was carried out using FastStart Universal SYBR Green Master (Roche, Basel, Switzerland) on a StepOnePlus™ real-time PCR system (Applied Biosystems, Foster City, CA, USA). PCR conditions were as follows: pre-incubation at 95 °C for 10 min, followed by 40 cycles of denaturation at 95 °C for 30 s, annealing at 55 °C for 30 s, and extension at 72 °C for 20 s. Triplicates were used for all analyses. Relative gene expression levels were normalized against that of the wild type and calculated against the 16S rRNA gene as the internal reference using the $2^{-\Delta\Delta Ct}$ method (Song et al. 2016; Livak and Schmittgen 2001). All primers used in the quantitative PCR assay are listed in Table S1.

PHA fermentation

PHA production by *P. mendocina* was carried out with a two-step fermentation process, including the stages of cell proliferation and PHA synthesis. Overnight culture (1%, *v*/*v*) was inoculated into 100 mL of NR medium (Wang et al. 2016) in a 500-mL flask and then incubated at 30 °C and 180 rpm for 24 h. The bacterial cells were harvested by centrifugation at 2500×*g* and 4 °C and resuspended in 1 mL PBS buffer. Then, the seed culture was inoculated into 100 mL of fermentation medium with 20 g/L glucose as the carbon source (pH 7.0) (Wang et al. 2016) in a 500-mL flask and cultivated at 30 °C and 180 rpm for 36 h. After shake-flask fermentation, the culture broth was centrifuged at 4 °C and 13,000×*g* for 20 min to collect the bacterial cells. Subsequently, the cells

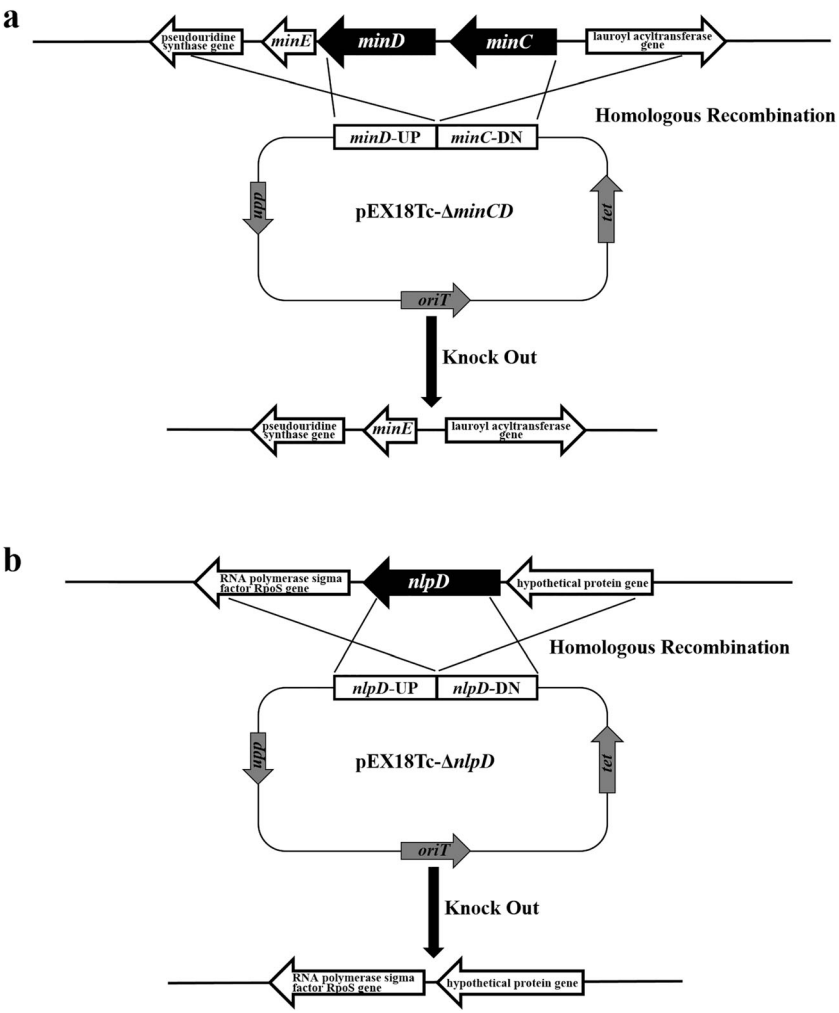

Fig. 1 The construction schematic diagram for knockout of *minCD* (**a**) and *nlpD* (**b**) in the genome of *P. mendocina* NKU

were lyophilized for 24 h and weighed. PHA was extracted from the lysed cells with chloroform at a rate of 100 mL chloroform/g cells at room temperature for 2 days. After being filtered to remove cellular debris, the extract containing PHA was concentrated by vacuum rotary evaporator. Then, a 40-fold volume of pre-cooled methanol was added to precipitate PHA overnight. The precipitate was re-dissolved in chloroform and the process was repeated to obtain the pure mcl-PHA. Finally, PHA was weighed after being dried at room temperature to remove all residual solvent (Guo et al. 2011a).

Results

Knockout and overexpression of cell morphologically related genes in *P. mendocina*

In *P. mendocina* NKU, *minC* and *minD* are located together in a gene cluster. In this work, *minCD* was deleted using the suicide plasmid in combination with *upp* as a counter-selectable marker. Additionally, *nlpD*, which activates amidases to regulate cell division, was also deleted in *P. mendocina* NKU (Fig. S2).

Compared with NKU pBBR, the transcriptional levels of *mreB* in NKU pBBR-*mreB* and NKU pBBR-*mreB-ftsZ* were improved by 340- and 441-fold, respectively. In NKU-Δ*minCD* pBBR-*mreB* and NKU-Δ*minCD* pBBR-*mreB-ftsZ*, the transcriptional levels of *mreB* had a 90- and 253-fold increase, respectively, compared with NKU-Δ*minCD* pBBR (Fig. 2a). The transcriptional levels of *ftsZ* in NKU pBBR-*ftsZ* and NKU pBBR-*mreB-ftsZ* had a 256- and 172-fold increase, respectively, compared with NKU pBBR. However, the transcriptional levels of *ftsZ* in NKU-Δ*minCD* pBBR-*ftsZ* and NKU-Δ*minCD* pBBR-*mreB-ftsZ* only had a 12- and 13-fold increase, respectively, compared with NKU-Δ*minCD* pBBR (Fig. 2b). The transcriptional levels of *sulA* in NKU pBBR-*sulA* and NKU-Δ*minCD* pBBR-*sulA* were improved by 102- and 23-fold, respectively, compared with NKU pBBR and NKU-Δ*minCD* pBBR (Fig. 2c). These results indicated that the transcription of the cell morphologically related genes was upregulated in *P. mendocina*.

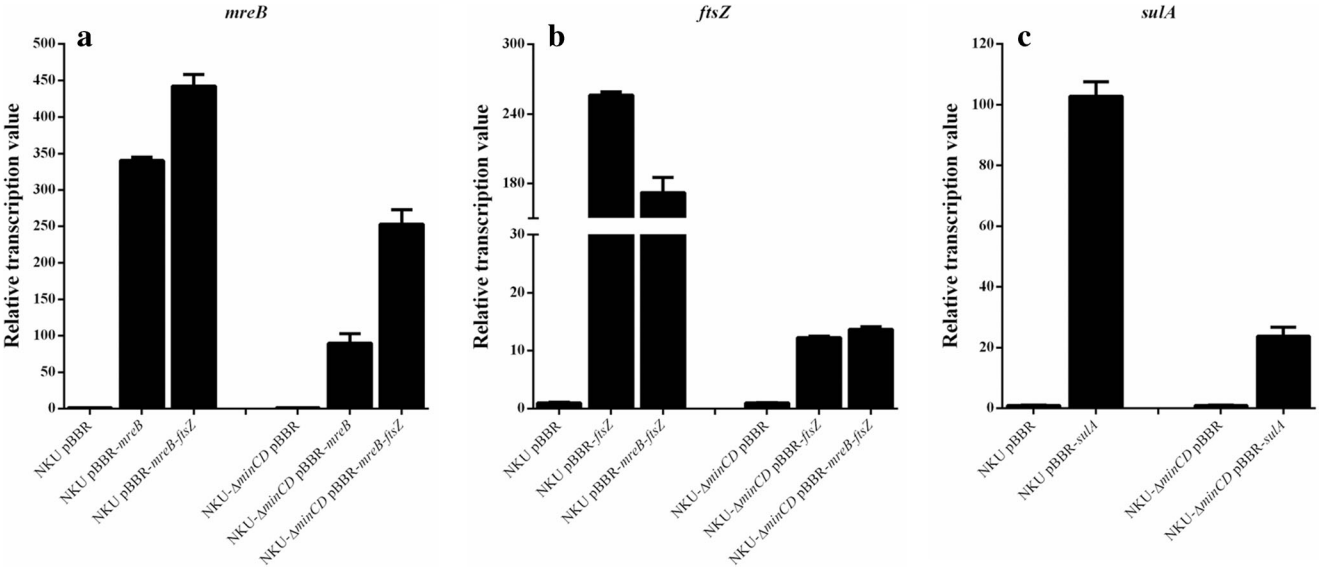

Fig. 2 qPCR analysis for the recombinant strains and *P. mendocina* NKU. Transcriptional levels of *mreB* (**a**), *ftsZ* (**b**), and *sulA* (**c**) for the different strains. The transcriptional levels for the control strains NKU pBBR and NKU-Δ*minCD* pBBR were set as 1. Error bars indicate the standard deviations. Data represent the mean values ± standard deviations of triplicate measurements from three independent experiments.

Effects of *minCD* and *nlpD* knockout on cell morphology and mcl-PHA accumulation

Pseudomonas mendocina NKU-Δ*minCD* showed a much longer cell length than the wild type when cultivated in LB medium (Fig. 3a). The average cell length of *P. mendocina* NKU-Δ*minCD* approached 3 μm and the longest was up to 10 μm, while the wild type was only 1.39 μm (Table 2). Moreover, the cells of NKU-Δ*minCD* presented different lengths and some min-cells were observed (Fig. 3a).

The log phase of NKU-Δ*minCD* was longer than NKU. However, the wild type early went into the decline phase than

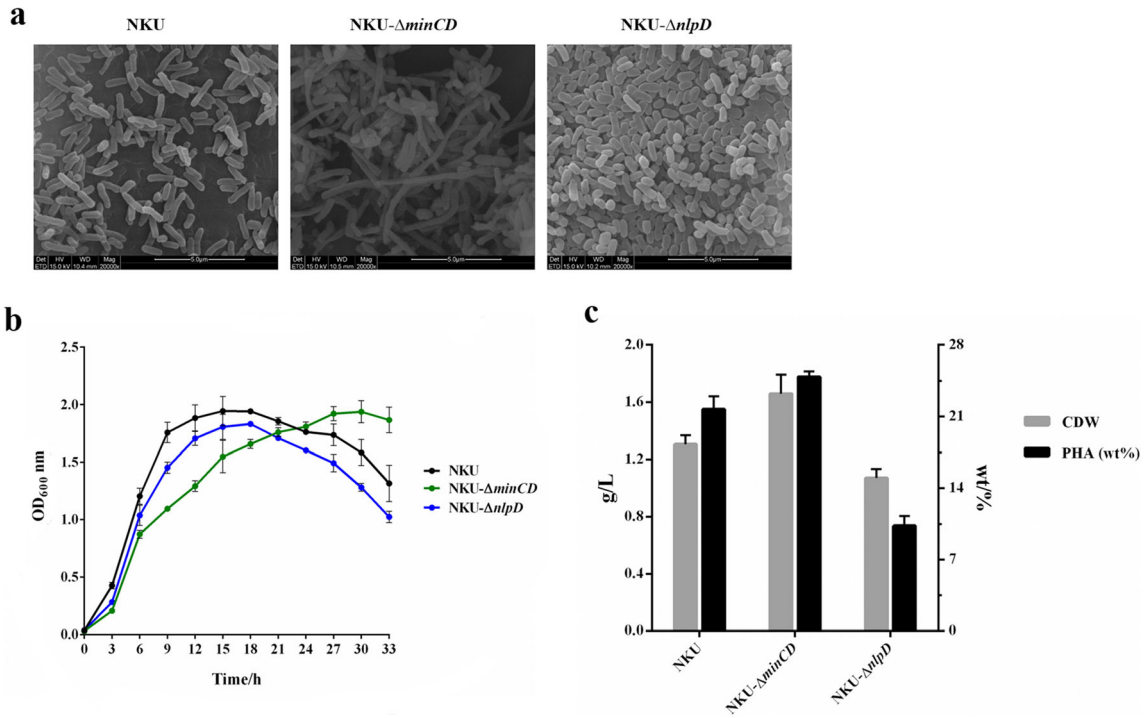

Fig. 3 Cell morphology (**a**), cell growth (**b**), and PHA production (**c**) of *P. mendocina* NKU, NKU-Δ*minCD*, and NKU-Δ*nlpD*. Samples for SEM were taken at stationary growth phase in LB medium. Scale bar, 5 μm. Cell growth was measured in LB medium at different growth phases. PHA production was performed in PHA fermentation medium. wt.% was defined as the ratio of PHA to CDW. Data represent the mean values ± standard deviations of triplicate measurements from three independent experiments.

Table 2 Cell size of *P. mendocina* NKU and its mutant strains in LB medium

Strains	Average cell length (μm)	Average cell width (μm)
P. mendocina NKU	1.39 ± 0.27	0.37 ± 0.03
P. mendocina NKU-Δ*minCD*	2.83 ± 2.04	0.37 ± 0.04
P. mendocina NKU-Δ*nlpD*	0.87 ± 0.19	0.45 ± 0.06
P. mendocina NKU pBBR	1.45 ± 0.20	0.39 ± 0.03
P. mendocina NKU pBBR-*mreB*	1.04 ± 0.20	0.54 ± 0.20
P. mendocina NKU pBBR-*ftsZ*	1.26 ± 0.32	0.38 ± 0.04
P. mendocina NKU pBBR-*sulA*	1.64 ± 0.43	0.39 ± 0.04
P. mendocina NKU pBBR-*mreB-ftsZ*	Multi-shaped	Multi-shaped
P. mendocina NKU-Δ*minCD* pBBR	2.41 ± 1.07	0.37 ± 0.04
P. mendocina NKU-Δ*minCD* pBBR-*mreB*	2.41 ± 1.28	0.42 ± 0.04
P. mendocina NKU-Δ*minCD* pBBR-*ftsZ*	1.60 ± 0.47	0.38 ± 0.03
P. mendocina NKU-Δ*minCD* pBBR-*sulA*	2.27 ± 1.13	0.36 ± 0.04
P. mendocina NKU-Δ*minCD* pBBR-*mreB-ftsZ*	Multi-shaped	Multi-shaped

did NKU-Δ*minCD* (Fig. 3b). Compared with the wild type, the CDW of NKU-Δ*minCD* was increased by 27% and the mcl-PHA yield of NKU-Δ*minCD* was increased by 45.62% from 0.28 to 0.41 g/L (i.e., from 21.67 to 24.87 wt.%) (Table S2 and Fig. 3c). The mcl-PHA yield (g/L) of all strains used in this study is listed in Table S2.

Compared with *P. mendocina* NKU, NKU-Δ*nlpD* had a shorter cell length and an increased cell width (Fig. 3a and Table 2). NKU-Δ*nlpD* showed a relatively poor growth (Fig. 3b). Compared with NKU, the CDW and PHA titer of NKU-Δ*nlpD* were decreased by 18% and 11%, respectively (Fig. 3c). Knockout of *nlpD* in *P. mendocina* NKU had a negative influence on cell growth and PHA production.

Effects of MreB, FtsZ, and SulA overexpression on cell morphology and mcl-PHA accumulation

Overexpression of *mreB* in *P. mendocina* NKU led to the formation of wider cells (Fig. 4a). The average cell width of NKU pBBR-*mreB* was 0.54 μm and the widest was up to 0.9 μm when cultivated in LB medium, while NKU pBBR had only a cell width of 0.39 μm (Table 2). The cell length of NKU pBBR-*mreB* was obviously shorter than that of NKU pBBR, and the cell shape was changed from rod to spherical shape (Fig. 4a). However, overexpression of *mreB* in NKU had a negative influence on cell growth, as shown by the growth curve in LB medium (Fig. 4b). The improvements in the PHA titer and CDW were also not observed with the *mreB*-overexpressing strain (Fig. 4c).

When *ftsZ* was overexpressed in NKU, some cells formed multi-FtsZ rings during the cell division (Fig. 4a) and the cell length was shortened (Fig. 4a and Table 2). Compared with NKU pBBR, the CDW of NKU pBBR-*ftsZ* was increased by 23.26% and the mcl-PHA yield of NKU pBBR-*ftsZ* was increased by 60.87% from 0.23 to 0.37 g/L (from 18.09 to 23.69 wt.%) (Fig. 4c and Table S2). For the *sulA*-overexpressing NKU strain, some longer cells were observed and the average cell length was changed from 1.45 to 1.64 μm (Fig. 4a and Table 2). The CDW and PHA titer of NKU pBBR-*sulA* had slight improvements compared with NKU pBBR (Fig. 4c). The growth of NKU pBBR-*ftsZ* and NKU pBBR-*sulA* had not a significant improvement compared with NKU pBBR (Fig. 4b). Unexpectedly, the cells of NKU pBBR-*mreB-ftsZ* were revealed to have different degrees of size expansion and irregular shapes. Many cells also became broken, resulting in cracked cell morphology (Fig. 4a). The cell growth and PHA accumulation also had an evident decrease (Fig. 4b, c).

Overexpression of *mreB*, *ftsZ*, and *sulA* in *P. mendocina* NKU Δ*minCD* for improved mcl-PHA production

When *mreB* overexpression in NKU-Δ*minCD*, the cell length maintained the elongated cell shape and the cell width was increased from 0.37 to 0.42 μm (Fig. 5a and Table 2). NKU-Δ*minCD* pBBR-*mreB* produced PHA accounting for 18.83% of CDW, which was higher than that (15.92%) of NKU-Δ*minCD* pBBR (Fig. 5c). Although the cell size of NKU-Δ*minCD* pBBR-*mreB* was larger than that of NKU-Δ*minCD* pBBR (Fig. 5b), the obtained CDW did not improve compared with NKU-Δ*minCD* pBBR.

When *ftsZ* was overexpressed in NKU-Δ*minCD*, the cell length was decreased from 2.41 to 1.60 μm compared with NKU-Δ*minCD*, and the different lengths of cells were observed for NKU-Δ*minCD* pBBR-*ftsZ* (Fig. 5a). The mcl-PHA accumulation in *ftsZ*-overexpressing NKU-Δ*minCD* was increased from 15.92 to 19.05 wt.% compared with NKU-Δ*minCD* pBBR (Fig. 5c).

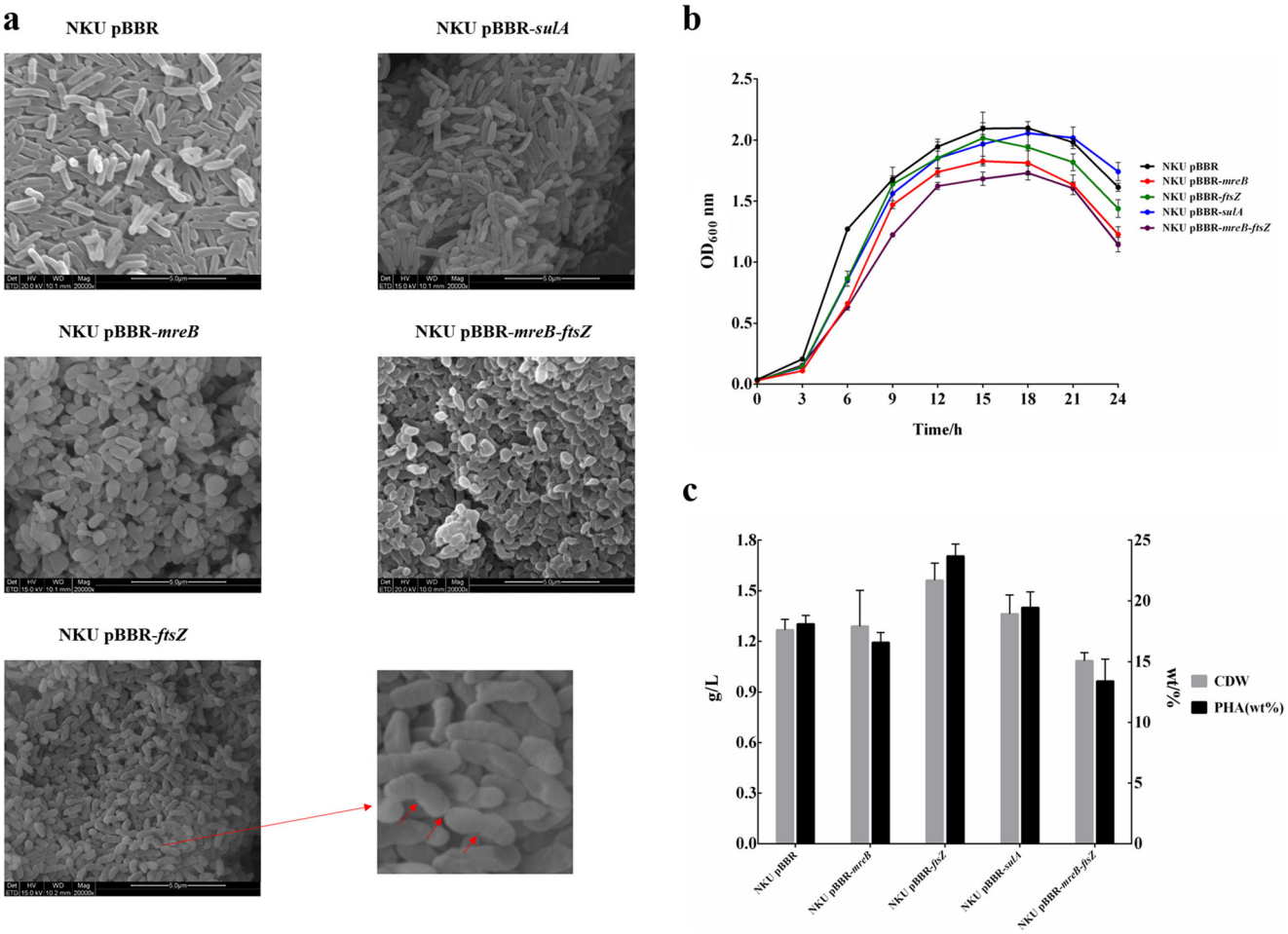

Fig. 4 Cell morphology (**a**), cell growth (**b**), and PHA production (**c**) of *P. mendocina* NKU pBBR, NKU pBBR-*mreB*, NKU pBBR-*ftsZ*, NKU pBBR-*sulA*, and NKU pBBR-*mreB-ftsZ*. Samples for SEM were taken at stationary growth phase in LB medium. Red arrows show more than one FtsZ rings in a dividing cell of NKU pBBR-*ftsZ*. Scale bar, 5 μm. Cell growth was measured in LB medium at different growth phases. PHA production was performed in PHA fermentation medium. wt.% was defined as the ratio of PHA to CDW. Data represent the mean values ± standard deviations of triplicate measurements from three independent experiments.

When NKU-Δ*minCD* harboring the plasmid pBBR-*mreB-ftsZ* was cultivated in LB medium, cell growth was obviously inhibited. Moreover, the cell morphology presented irregular cell shapes and even some cracked cells were generated, which were also observed with NKU pBBR-*mreB-ftsZ* (Fig. 4a). Co-overexpression of *mreB* and *ftsZ* in NKU-Δ*minCD* also had the influence on the mcl-PHA titer decreasing from 15.92 to 10.74 wt.% and on the CDW decreasing from 1.29 to 0.9 g/L compared with NKU-Δ*minCD* pBBR (Fig. 5c).

The *ftsZ* inhibitor, SulA, was overexpressed in NKU-Δ*minCD* to investigate the influence on mcl-PHA production and cell morphology. As shown in Fig. 5, cells of NKU-Δ*minCD* pBBR-*sulA* maintained the long filamentary status in LB medium. The cell length had not a significant change in comparison with NKU-Δ*minCD* pBBR. Nevertheless, the mcl-PHA accumulation had a slight increase and the CDW had a reduction (Fig. 5c).

Discussion

Inclusion bodies accumulated by many bacteria can be used in industrial applications, such as PHAs which can be used as biodegradable materials. Many different methods have been used to enhance the production of PHAs, such as metabolic engineering, synthetic biology, and the use of cheap substrates (Poblete-Castro et al. 2013; Borrero-de Acuña et al. 2014; Wang et al. 2016; Fontaine et al. 2017). Recently, morphology engineering which could change the cell size and cell division pattern to increase the PHB accumulation (Jiang and Chen 2016) has attracted many attentions. In this study, many cell morphology genes of *P. mendocina* NKU were manipulated to change the cell size and enhance the mcl-PHA synthesis.

MinCD inhibits the formation of FtsZ ring. It has been shown that overexpression of *minCD* in *E. coli* generated filament cells due to the absence of FtsZ rings (Bi and Lutkenhaus 1993). Conversely, deletion of *minCD* resulted

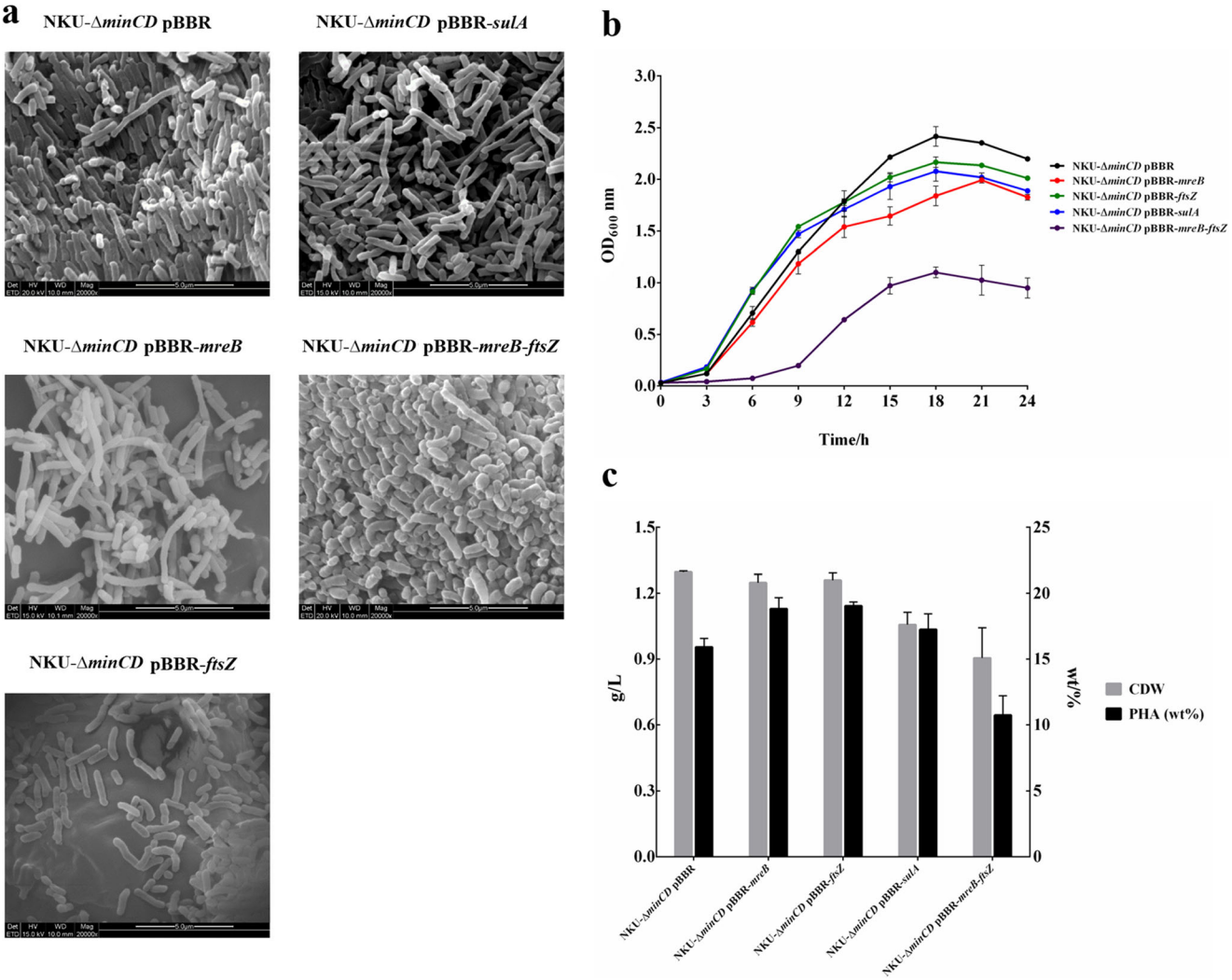

Fig. 5 Cell morphology (**a**), cell growth (**b**), and PHA production (**c**) of *P. mendocina* NKU-Δ*minCD* pBBR, NKU-Δ*minCD* pBBR-*mreB*, NKU-Δ*minCD* pBBR-*ftsZ*, NKU-Δ*minCD* pBBR-*sulA*, and NKU-Δ*minCD* pBBR-*mreB-ftsZ*. Samples for SEM were taken at stationary growth phase in LB medium. Scale bar, 5 μm. Cell growth was measured in LB medium at different growth phases. PHA production was performed in PHA fermentation medium. wt.% was defined as the ratio of PHA to CDW. Data represent the mean values ± standard deviations of triplicate measurements from three independent experiments.

in the formation of FtsZ rings in any position of a cell (Zhou and Lutkenhaus 2005) and the generation of elongated cells (Wu et al. 2016a). The cell division way of the *minCD* knockout mutant was changed from binary fission to multiple fission process (Wu et al. 2016a). In this study, many cells became much longer after *minCD* was deleted in *P. mendocina* NKU (Fig. 3a). Since the FtsZ ring was located in any position of a cell for NKU-Δ*minCD*, the division pattern was changed from binary division to multiple fission and the imbalanced division led to the formation of different lengths of cells, including elongated cells and min cells. Except for the change of cell morphology, NKU-Δ*minCD* had improvements in the mcl-PHA titer and CDW compared with NKU, which may give the credit to the larger cell size allowing the accumulation of more PHA granules (Fig. 3c).

The two essential genes *mreB* and *ftsZ* play important roles in controlling the cell length and width, respectively (Elhadi et al. 2016). Although the bacteria with deletion of *mreB* or *ftsZ* displayed larger spherical cell shape and formed longer cells, they showed poor cell growth and reduced PHB production (Jiang et al. 2015, 2017). In this research, the cells were changed from rod to spherical shape when *mreB* was overexpressed in *P. mendocina* NKU (Fig. 4a). The reason may be that the high expression level of MreB strengthened the extensibility of the bacterial cytoskeletons. Interestingly, some min rod cells were also found for *mreB* overexpression (Fig. 4a), suggesting that the stability of NKU pBBR-*mreB* may need to be improved. NKU pBBR-*mreB* showed poor cell growth compared with NKU pBBR (Fig. 4b); thus, there were no improvements in the PHA titer and CDW for *mreB*-overexpressing NKU (Fig. 4c).

It was reported that *ftsZ* overexpression could accelerate cell division (Wang and Lee 1997). More than one FtsZ rings in a dividing cell were appeared due to increased quantities of FtsZ when *ftsZ* was overexpressed in *P. mendocina* NKU (Fig. 4a). The cell length was shortened after the occurrence of binary division more than once for a normal cell (Fig. 4a). The CDW and mcl-PHA titer were improved for NKU pBBR-*ftsZ* (Fig. 4c), suggesting that the formed multiple FtsZ rings may accelerate the binary division of a cell, resulting in higher CDW and more PHA accumulation.

Unfortunately, the cells with simultaneous overexpression of *mreB* and *ftsZ* showed poor cell growth (Fig. 4b) and multiple-shaped cells (Fig. 4a). Both the CDW and mcl-PHA titer had an obvious decrease (Fig. 4c). It seemed that the normal cell division was destructed when a spherical shape cell contained more than one FtsZ rings. Many cells presented irregular shapes and cracked cell morphology (Fig. 4a).

The *mreB* or *ftsZ* gene was also overexpressed in NKU-Δ*minCD*. Although the elongated cells were obtained by knockout of *minCD*, the cell width had not an enhancement as well as some min-cells appeared. However, overexpression of *mreB* in NKU led to the formation of spherical shape cells. It was expected that the elongated cells of NKU-Δ*minCD* would be widen along with *mreB* overexpression. The cells of NKU-Δ*minCD* pBBR-*mreB* maintained the elongated cell shape, and the increase in the cell width was also observed (Fig. 5a and Table 2). Moreover, the mcl-PHA titer was increased from 15.92 to 18.83 wt.% compared with NKU-Δ*minCD* pBBR (Fig. 5c). However, the CDW of *mreB*-overexpressing NKU-Δ*minCD* did not show an increase, possibly resulting from poor cell growth. It should be noted that the CDW of NKU pBBR-*mreB* and NKU-Δ*minCD* pBBR-*mreB* independently maintained the similar levels to NKU pBBR and NKU-Δ*minCD* pBBR, even though poor cell growth occurred in both of the two strains. These results indicated that cell morphology affected the relationship between dry biomass and optical density and that the cell dry biomass was determined by both cell morphology and optical density.

Since the location of FtsZ ring on the cell for NKU-Δ*minCD* was uncontrollable, the elongated cell needed more FtsZ rings to achieve the multiple division. The NKU-Δ*minCD* cells with *ftsZ* overexpression did not maintain the elongated cell shape in LB medium (Fig. 5a). This phenomenon indicated that the multiple division was accelerated for the elongated cell harboring more than one FtsZ rings and finally realized in NKU-Δ*minCD* pBBR-*ftsZ*. The results indicated that individual overexpression of *ftsZ* and *mreB* in NKU-Δ*minCD* could accelerate the cell division process and enlarge the cell size.

In this work, *mreB* and *ftsZ* were also simultaneously overexpressed in NKU-Δ*minCD* to investigate the effects of co-expression on cell shape and mcl-PHA production. As the cell morphology of NKU pBBR-*mreB-ftsZ*, it presented spherical shapes and many cells seemed cracked (Fig. 5a). The cell growth and mcl-PHA production were seriously affected (Fig 5b, c). It has been shown that cell growth and PHB production were improved by overexpressing gene *ftsZ* together with cytoskeleton protein gene *mreB* in *E. coli* JM109 Δ*minCD* (Wu et al. 2016a). However, co-overexpression of *mreB* and *ftsZ* in NKU-Δ*minCD* not only did not accelerate cell division and increase cell size but also led to unhealthy cell growth and appeared cracked cells. In *E. coli*, knockout of *nlpD* gene led to elongated cells (Wu et al. 2016b), but the cells became shorter by deleting the *nlpD* gene in NKU. These results suggest that the same cell morphology genes may have different roles in different bacteria. Currently, morphology engineering is not an exactly controllable pattern. To precisely manipulate the change of cell morphology, more in-depth studies for the cell morphology genes are needed in the future.

Previous reports revealed that overexpression of a FtsZ inhibitor SulA inhibits cell division to produce long and non-septate filaments (Chen et al. 2012; Wu et al. 2016b; Wang et al. 2014). In this study, the *sulA* gene was overexpressed, respectively, in NKU and NKU-Δ*minCD*. However, the cell length for NKU pBBR-*sulA* did not show an obvious increase compared with the inducible overexpression of *sulA* in *E. coli* (Wu et al. 2016b). These results indicated that the cell division could be slightly inhibited by *sulA* overexpression in *P. mendocina*. In addition, the NKU pBBR-*sulA* cells may not maintain lengthy shapes over the entire growth period, while the SEM samples derived from stationary phase cultures might not be optimal for the observation of lengthy cells. Anyhow, overexpression of *sulA* in NKU and NKU-Δ*minCD* had slight enhancements for mcl-PHA accumulation (Figs. 4c and 5c). These results suggest that an appropriate quantity of SulA may be important for maintaining the cell length.

The NKU-Δ*minCD* pBBR cells did not show an obvious elongation when cultured in fermentation medium (Fig. S3). Moreover, the cell shapes of NKU-Δ*minCD* pBBR-*mreB* and NKU-Δ*minCD* pBBR-*sulA* in fermentation medium were also not as long as that observed in LB medium (Fig. S3). Compared with NKU-Δ*minCD* pBBR, the recombinant strains NKU-Δ*minCD* pBBR-*mreB*, NKU-Δ*minCD* pBBR-*ftsZ*, and NKU-Δ*minCD* pBBR-*sulA* had the increased average cell length and width when cultured in fermentation medium (Table S3). The increases in cell size were positively related to the mcl-PHA titers obtained with the recombinant strains. The mcl-PHA titers were improved by overexpression of *mreB*, *ftsZ*, or *sulA* in NKU-Δ*minCD* (Fig. 5c). It is speculated that the cell shape may be dependent on many factors such as cell morphologically related genes and the culture conditions.

Morphology engineering should open up a new avenue for enhanced PHA production by manipulating cell shape–related genes. This strategy has been used to improve PHB

accumulation in *E. coli* and *Halomonas*. However, PHB is brittle and stiff due to its high T_m (> 170 °C) (Ouyang et al. 2007; Noda et al. 2004, 2005; Li et al. 2007). mcl-PHA normally contain monomer units of 3-hydroxyhexanoate (3HHx), 3-hydroxyoctanoate (3HO), 3-hydroxydecanoate (3HD), and 3-hydroxydodecanoate (3HDD). mcl-PHA are elastomeric with longer elongation rate due to their low T_m. Thus, mcl-PHA can be used as biodegradable elastomers, adhesives, or blending materials to improve the physical properties of PHAs. In summary, the mcl-PHA production was enhanced by manipulating the cell morphologically related genes in *P. mendocina* NKU. To our knowledge, this is the first report on the improvement of mcl-PHA synthesis by cell morphology engineering. Many bacteria from the genus *Pseudomonas* have an ability to produce various mcl-PHA. This study provides an alternative strategy to enhance the mcl-PHA accumulation in these bacteria.

It should be noted that the mcl-PHA production of *P. mendocina* NKU did not have a significant increase as the PHB synthesis of recombinant *E. coli* (Wu et al. 2016a, b; Elhadi et al. 2016) by engineering cell morphology. There could be many reasons. Firstly, *P. mendocina* NKU is a mcl-PHA production strain which was isolated by our laboratory. The mcl-PHA synthetic ability for *pseudomonas* may not as strong as that of PHB accumulation for recombinant *E. coli*. In addition, morphology engineering may bring changes in metabolism which may be the second reason for the enhancement of PHA. And the metabolic network of *E. coli* was simpler than that of *pseudomonas*. Therefore, the impacts for mcl-PHA accumulation of NKU and PHB accumulation of recombinant *E. coli* by morphology engineering had a difference.

Morphology engineering has been an effective method to accelerate cell growth, simplify downstream separation, and enlarge space for more inclusion body accumulation (Jiang and Chen 2016). Up to now, only limited genes such as *ftsZ*, *sulA*, *minCD*, and *mreB* have been investigated to change the cell morphology. Many genes such as *ftsA*, *mbl*, *rodZ*, and *rodA* have not yet been applied for engineering the cell morphology (Jiang and Chen 2016). It is also necessary to exploit new engineering solutions for precisely controlling the change of cell shape. Morphology engineering also possesses the potential to improve the production of other bio-chemicals (Gao et al. 2016) and is a promising approach to construct microbial cell factories in combination with metabolic engineering.

In this study, the mcl-PHA accumulation in *P. mendocina* NKU was enhanced by manipulating cell morphology and cell division pattern through the deletion and overexpression of cell morphologically related genes. Thus, morphology engineering may be a feasible method to improve the production of cellular inclusion bodies and other valuable bio-based products.

Funding information This work was financially supported by the National Natural Science Funding of China (Grant Nos. 31470213, 31570035 and 31670093), the Tianjin Natural Science Funding (Grant Nos. 17JCZDJC32100 and 18JCYBJC24500), and the Postdoctoral Science Funding of China (Grant No. 2018M631729).

Compliance with ethical standards

Conflict of interest The authors declare that they have no conflict of interest.

Ethical approval This article does not contain any studies with human participants or animals performed by any of the authors.

Publisher's Note Springer Nature remains neutral with regard to jurisdictional claims in published maps and institutional affiliations.

References

Anderson DE, Gueiros-Filho FJ, Erickson HP (2004) Assembly dynamics of FtsZ rings in *Bacillus subtilis* and *Escherichia coli* and effects of FtsZ-regulating proteins. J Bacteriol 186:5775–5781

Bi E, Lutkenhaus J (1993) Cell division inhibitors SulA and MinCD prevent formation of the FtsZ ring. J Bacteriol 175:1118–1125

Borrero-de Acuña JM, Bielecka A, Häussler S, Schobert M, Jahn M, Wittmann C, Jahn D, Poblete-Castro I (2014) Production of medium chain length polyhydroxyalkanoate in metabolic flux optimized *Pseudomonas putida*. Microb Cell Factories 13:88

Boyle DS, Khattar MM, Addinall SG, Lutkenhaus J, Donachie WD (1997) *ftsW* is an essential cell-division gene in *Escherichia coli*. Mol Microbiol 24:1263–1273

Cabeen MT, Jacobs-Wagner C (2010) The bacterial cytoskeleton. Annu Rev Genet 44:365–392

Chen GQ (2009) A microbial polyhydroxyalkanoates (PHA) based bio- and materials industry. Chem Soc Rev 38:2434–2446

Chen GQ, Wu Q (2005) The application of polyhydroxyalkanoates as tissue engineering materials. Biomaterials 26:6565–6578

Chen Y, Milam S, Erickson H (2012) SulA inhibits assembly of FtsZ by a simple sequestration mechanism. Biochemistry 51:3100–3109

Chung AL, Zeng GD, Jin HL, Wu Q, Chen JC, Chen GQ (2013) Production of medium-chain-length 3-hydroxyalkanoic acids by β-oxidation and *phaC* operon deleted *Pseudomonas entomophila* harboring thioesterase gene. Metab Eng 17:23–29

Dajkovic A, Mukherjee A, Lutkenhaus J (2008) Investigation of regulation of FtsZ assembly by SulA and development of a model for FtsZ polymerization. J Biotechnol 190:2513–2526

den Blaauwen T, de Pedro MA, Nguyen-Disteche M, Ayala JA (2008) Morphogenesis of rod-shaped sacculi. FEMS Microbiol Rev 32: 321–344

Elhadi D, Lv L, Jiang XR, Wu H, Chen GQ (2016) CRISPRi engineering *E. coli* for morphology diversification. Metab Eng 38:358–369

Feng J, Gao W, Gu Y, Zhang W, Cao M, Song C, Zhang P, Sun M, Yang C, Wang S (2014) Functions of poly-gamma-glutamic acid (γ-PGA) degradation genes in γ-PGA synthesis and cell morphology maintenance. Appl Microbiol Biotechnol 98:6397–6407

Fontaine P, Mosrati R, Corroler D (2017) Medium chain length polyhydroxyalkanoates biosynthesis in *Pseudomonas putida* mt-2 is enhanced by co-metabolism of glycerol/octanoate or fatty acids mixtures. Int J Biol Macromol 98:430–435

Gao X, Chen JC, Wu Q, Chen GQ (2011) Polyhydroxyalkanoates as a source of chemicals, polymers, and biofuels. Curr Opin Biotechnol 22:768–774

Gao W, Zhang Z, Feng J, Dang Y, Quan Y, Gu Y, Wang S, Song C (2016) Effects of MreB paralogs on poly-γ-glutamic acid synthesis and cell morphology in *Bacillus amyloliquefaciens*. FEMS Microbiol Lett 363:fnw187

Gitai Z (2005) The new bacterial cell biology: moving parts and subcellular architecture. Cell 120:577–586

Green MR, Sambrook J (2012) Molecular cloning: a laboratory manual, 4th edn. Cold Spring Harbor Laboratory Press, Cold Spring Harbor

Guo W, Song C, Kong M, Geng W, Wang Y, Wang S (2011a) Simultaneous production and characterization of medium-chain-length polyhydroxyalkanoates and alginate oligosaccharides by *Pseudomonas mendocina* NK-01. Appl Microbiol Biotechnol 92: 791–801

Guo W, Wang Y, Song C, Yang C, Li Q, Li B, Su W, Sun X, Song D, Yang X, Wang S (2011b) Complete genome of *Pseudomonas mendocina* NK-01, which synthesizes medium-chain-length polyhydroxyalkanoates and alginate oligosaccharides. J Bacteriol 193:3413–3414

Higashitani A, Higashitani N, Horiuchi K (1995) A cell division inhibitor SulA of *Escherichia coli* directly interacts with FtsZ through GTP hydrolysis. Biochem Biophys Res Commun 209:198–204

Howard M (2004) A mechanism for polar protein localization in bacteria. J Mol Biol 335:655–663

Ivanov V, Mizuuchi K (2010) Multiple modes of interconverting dynamic pattern formation by bacterial cell division proteins. Proc Natl Acad Sci U S A 107:8071–8078

Jiang XR, Chen GQ (2016) Morphology engineering of bacteria for bioproduction. Biotechnol Adv 34:435–440

Jiang XR, Wang H, Shen R, Chen GQ (2015) Engineering the bacterial shapes for enhanced inclusion bodies accumulation. Metab Eng 29: 227–337

Jiang XR, Yao ZH, Chen GQ (2017) Controlling cell volume for efficient PHB production by *Halomonas*. Metab Eng 44:30–37

Kovach ME, Elzer PH, Hill DS, Robertson GT, Farris MA, Roop RMII, Peterson KM (1995) Four new derivatives of the broad-host-range cloning vector pBBR1MCS, carrying different antibiotic-resistance cassettes. Gene 166:175–176

Li R, Zhang H, Qi Q (2007) The production of polyhydroxyalkanoates in recombinant *Escherichia coli*. Bioresour Technol 98:2313–2320

Liu Q, Luo G, Zhou XR, Chen GQ (2011) Biosynthesis of poly(3-hydroxydecanoate) and 3-hydroxydodecanoate dominating polyhydroxyalkanoates by beta-oxidation pathway inhibited *Pseudomonas putida*. Metab Eng 13:11–17

Livak KJ, Schmittgen TD (2001) Analysis of relative gene expression data using real-time quantitative PCR and the 2(-Delta Delta C(T)) Method. Methods 25:402–408

Loose M, Mitchison TJ (2014) The bacterial cell division proteins FtsA and FtsZ self-organize into dynamic cytoskeletal patterns. Nat Cell Biol 16:38–46

Ma L, Zhang H, Liu Q, Chen J, Zhang J, Chen GQ (2009) Production of two monomer structures containing medium-chain-length polyhydroxyalkanoates by beta-oxidation-impaired mutant of *Pseudomonas putida* KT2442. Bioresour Technol 100:4891–4894

Margolin W (2005) FtsZ and the division of prokaryotic cells and organelles. Nat Rev Mol Cell Biol 6:862–871

Noda I, Satkowski MM, Dowrey AE, Marcott C (2004) Polymer alloys of Nodax copolymers and poly(lactic acid). Macromol Biosci 4:269–275

Noda I, Green PR, Satkowski MM, Schechtman LA (2005) Preparation and properties of a novel class of polyhydroxyalkanoate copolymers. Biomacromolecules 6:580–586

Ouyang SP, Luo RC, Chen SS, Liu Q, Chung A, Wu Q, Chen GQ (2007) Production of polyhydroxyalkanoates with high 3-hydroxydodecanoate monomer content by *fadB* and *fadA* knockout mutant of *Pseudomonas putida* KT2442. Biomacromolecules 8: 2504–2511

Pichoff S, Lutkenhaus J (2001) *Escherichia coli* division inhibitor MinCD blocks septation by preventing Z-ring formation. J Bacteriol 183:6630–6635

Poblete-Castro I, Binger D, Rodrigues A, Becker J, Martins Dos Santos VA, Wittmann C (2013) In-silico-driven metabolic engineering of *Pseudomonas putida* for enhanced production of poly-hydroxyalkanoates. Metab Eng 15:113–123

Reddy CS, Ghai R, Rashmi, Kalia VC (2003) Polyhydroxyalkanoates: an overview. Bioresour Technol 87:137–146

Rowlett VW, Margolin W (2013) The bacterial Min system. Curr Biol 23: R553–R556

Song Y, Nikoloff JM, Fu G, Chen J, Li Q, Xie N, Zheng P, Sun J, Zhang D (2016) Promoter screening from *Bacillus subtilis* in various conditions hunting for synthetic biology and industrial applications. PLoS One 11:e0158447

Tan D, Wu Q, Chen JC, Chen GQ (2014) Engineering *Halomonas* TD01 for low cost production of polyhydroxyalkanoates. Metab Eng 26:34–47

Tao W, Lv L, Chen GQ (2017) Engineering *Halomonas* species TD01 for enhanced polyhydroxyalkanoates synthesis via CRISPRi. Microb Cell Factories 16:48

Uehara T, Dinh T, Bernhardt TG (2009) LytM-domain factors are required for daughter cell separation and rapid ampicillin-induced lysis in *Escherichia coli*. J Bacteriol 191:5094–5107

Uehara T, Parzych KR, Dinh T, Bernhardt TG (2010) Daughter cell separation is controlled by cytokinetic ring-activated cell wall hydrolysis. EMBO J 29:1412–1422

Van den Ent F, Amos LA, Löwe J (2001) Prokaryotic origin of the actin cytoskeleton. Nature 413:39–44

Villanelo F, Ordenes A, Brunet J, Lagos R, Monasterio O (2011) A model for the *Escherichia coli* FtsB/FtsL/FtsQ cell division complex. BMC Struct Biol 11:28

Wang F, Lee SY (1997) Production of poly(3-hydroxybutyrate) by fed-batch culture of filamentation-suppressed recombinant *Escherichia coli*. Appl Environ Microbiol 63:4765–4769

Wang S, Arellano-Santoyo H, Combs PA, Shaevitz JW (2010) Actin-like cytoskeleton filaments contribute to cell mechanics in bacteria. Proc Natl Acad Sci U S A 107:9182–9185

Wang Y, Wu H, Jiang XR, Chen GQ (2014) Engineering *Escherichia coli* for enhanced production of poly(3-hydroxybutyrate-co-4-hydroxybutyrate) in larger cellular space. Metab Eng 25:183–193

Wang Y, Zhang C, Gong T, Zuo Z, Zhao F, Fan X, Yang C, Song C (2015) An upp-based markerless gene replacement method for genome reduction and metabolic pathway engineering in *Pseudomonas mendocina* NK-01 and *Pseudomonas putida* KT2440. J Microbiol Methods 113:27–33

Wang Y, Zhao F, Fan X, Wang S, Song C (2016) Enhancement of medium-chain-length polyhydroxyalkanoates biosynthesis from glucose by metabolic engineering in *Pseudomonas mendocina*. Biotechnol Lett 38:313–320

Ward JE Jr, Lutkenhaus J (1985) Overproduction of FtsZ induces minicell formation in *E. coli*. Cell 42:941–999

Wu H, Fan Z, Jiang X, Chen J, Chen GQ (2016a) Enhanced production of polyhydroxybutyrate by multiple dividing *E. coli*. Microb Cell Factories 27:15

Wu H, Chen JC, Chen GQ (2016b) Engineering the growth pattern and cell morphology for enhanced PHB production by *Escherichia coli*. Appl Microbiol Biotechnol 100:9907–9916

Zhou H, Lutkenhaus J (2005) MinC mutants deficient in MinD- and DicB-mediated cell division inhibition due to loss of interaction with MinD, DicB, or a septal component. J Bacteriol 187:2846–2857